

Protein Degradation

Sulfinyl Aziridines as Stereoselective Covalent Destabilizing Degraders of the Oncogenic Transcription Factor MYC

Hannah T. Rosen⁺, Kelvin Li⁺, Christian E. Stieger, Erin L. Li, Brynne Currier, Scott M. Brittain, Francisco J. Garcia, Diana C. Beard, Michael D. Jones, Sandra Haenni-Holzinger, Dustin Dovala, Jeffrey M. McKenna, Markus Schirle, Thomas J. Maimone,* and Daniel K. Nomura*

Abstract: Although MYC is a significant oncogenic transcription factor driver of cancer, directly targeting MYC has remained challenging due to its intrinsic disorder and poorly defined structure, deeming it “undruggable.” Whether transient pockets formed within unstructured regions of proteins can be selectively targeted with small molecules remains an outstanding challenge. Here, we developed a stereochemically paired spirocyclic oxindole aziridine covalent library and screened this library for degradation of MYC. We identified a hit covalent ligand, KL2-236, bearing a unique sulfinyl aziridine warhead, that engaged MYC as a pure MYC/MAX protein complex, and in cancer cells to destabilize MYC, inhibit MYC transcriptional activity and degrade MYC in a proteasome-dependent manner through targeting intrinsically disordered C203 and D205 residues. Notably, this reactivity was most pronounced for specific stereoisomers of KL2-236 with a diastereomer, KL4-019, that was largely inactive. Mutagenesis of both C203 and D205 completely attenuated KL2-236-mediated MYC degradation. We also optimized our KL2-236 hit compound to generate a more potent, selective, and durable MYC degrader, KL4-219A. Our results reveal a novel ligandable site within MYC and indicate that certain intrinsically disordered regions within transcription factors, such as MYC, can be interrogated by isomerically unique chiral small molecules, leading to destabilization and degradation.

Introduction

Among “undruggable” targets that have been identified, transcription factors have represented a particularly challenging class of targets for drug discovery due to the presence of large regions of intrinsic disorder and poorly defined structures for many members. Whether these unstructured regions of transcription factors have ligandable sites that can be pharmacologically targeted in a selective manner is often unclear.^[1]

MYC has been a particularly elusive target for direct targeting due to its high degree of intrinsic disorder and poorly defined structure.^[2–4] Several therapeutic strategies have indirectly targeted MYC or the MYC pathway. MYC

is a nuclear transcription factor that drives the expression of genes required for cell growth, metabolism, and survival, and it is one of the most frequently amplified oncogenes in human malignancies.^[2,5] Through required heterodimerization with MAX, MYC binds E-box sequences to activate its targets. Because of MYC’s key role in tumor development, extensive efforts have focused on developing agents that either block MYC directly or interfere with pathways that control it.^[2,3,6,7] Such strategies include impeding MYC transcription with bromodomain and extraterminal (BET) family inhibitors or CDK7/9 inhibitors,^[8] reducing MYC translation via mTORC1 or AKT/PI3K inhibitors,^[2,4] preventing MYC-MAX dimer formation,^[2,4] and inhibiting BRD4 with inhibitors such as

[*] H. T. Rosen⁺, K. Li⁺, C. E. Stieger, E. L. Li, B. Currier, T. J. Maimone, D. K. Nomura
Department of Chemistry, University of California, Berkeley, Berkeley, CA 94720, USA
E-mail: maimone@berkeley.edu
dnomura@berkeley.edu

H. T. Rosen⁺, C. E. Stieger, B. Currier, D. K. Nomura
Department of Molecular and Cell Biology, University of California, Berkeley, Berkeley, CA 94720, USA

H. T. Rosen⁺, C. E. Stieger, B. Currier, D. K. Nomura
Innovative Genomics Institute, Berkeley, CA 94720, USA

H. T. Rosen⁺, K. Li⁺, C. E. Stieger, E. L. Li, B. Currier, S. M. Brittain, F. J. Garcia, D. C. Beard, M. D. Jones, S. Haenni-Holzinger, D. Dovala, J. M. McKenna, M. Schirle, T. J. Maimone, D. K. Nomura


Novartis-Berkeley Translational Chemical Biology Institute, Berkeley, CA 94720, USA

S. M. Brittain, F. J. Garcia, D. C. Beard, M. D. Jones, S. Haenni-Holzinger, D. Dovala, J. M. McKenna, M. Schirle
Novartis Biomedical Research, Emeryville, CA, USA

S. M. Brittain, F. J. Garcia, D. C. Beard, M. D. Jones, S. Haenni-Holzinger, D. Dovala, J. M. McKenna, M. Schirle
Novartis Biomedical Research, Cambridge, MA, USA

S. M. Brittain, F. J. Garcia, D. C. Beard, M. D. Jones, S. Haenni-Holzinger, D. Dovala, J. M. McKenna, M. Schirle
Novartis Biomedical Research, Basel, Switzerland

[⁺] Both authors contributed equally to this work.

 Additional supporting information can be found online in the Supporting Information section

JQ1 and GSK525762 that disrupt BRD4 binding at acetylated chromatin regions necessary for MYC transcription. Small-molecule microarray approaches have also uncovered MAX/MAX homostabilizers that sequester MAX away from MYC, thereby impairing MYC's transcriptional function,^[9] and small-molecule inhibitors have been developed that disrupt the WDR5 and MYC protein interaction.^[10–13] Nevertheless, directly targeting MYC remains challenging due to its predominantly disordered structure and lack of prominent binding pockets, earning it the reputation of being “undruggable.”

Over the past several decades, covalent chemoproteomic approaches such as activity-based protein profiling (ABPP) have arisen as powerful approaches for uncovering unique, cryptic, allosteric, or shallow ligandable sites that can be accessed with covalently-acting small molecules through balancing reactivity with binding affinity.^[14–25] There have also been several successes in using covalent chemistry to target transcription factors, including against a palmitoylation site cysteine in the Hippo pathway transcription factor TEAD,^[26] a cysteine within the Wnt pathway transcription factor CTNBN1,^[22] and most recently, a cysteine in FOXA1 to rewire its transcriptional specificity.^[23] Recently, we have also uncovered a covalent ligand EN4 that targets an allosteric cysteine, C171 (or C186, depending on the MYC isoform and associated protein sequence) to cause destabilization of MYC and subsequent inhibition of MYC/MAX binding to DNA and MYC transcriptional activity in cells, leading to down-regulation of MYC target genes, and anti-proliferative and anti-tumorigenic effects.^[21] The Bar–Peled lab has also previously used covalent chemoproteomics profiling with scout ligands across a panel of cancer cell lines to identify ligandable sites across the proteome, including in MYC.^[24] Some of these covalent ligands, including EN4, have been shown to target intrinsically disordered cysteines within these proteins.^[21] However, whether there is an actionable binding pocket or non-covalent interactions recognized by these molecules versus whether the binding occurs mainly through reactivity-driven binding has been less clear. One strategy to begin to address this question is through the use of stereochemically matched compound libraries composed of either enantio- and/or diastereomerically matched compounds that allow the direct comparisons between these stereoisomers to determine if stereoselective interactions exist in the bioconjugation of the corresponding protein target with the electrophilic fragment. Previous studies from Cravatt, Vinogradova, and others have extensively exemplified such studies using various chemical scaffolds such as tryptoline-based acrylamides and spirocyclic acrylamides.^[18,23,27–31]

In this study, we discovered that spirocyclic oxindole-based sulfinyl aziridines can stereoselectively modulate MYC levels and thus inhibit MYC transcriptional activity in cells. We synthesized a small library of covalent ligands bearing electrophilic aziridine-derived warheads of variable reactivity coupled with stereochemical pairing. Through this effort, we identified and optimized a covalent ligand that directly engages an intrinsically disordered cysteine in MYC in a stereoselective manner and, as a result, leads to MYC

destabilization and proteasome-dependent degradation in cells.

Results

Synthesis and Screening of a Stereochemically Paired Covalent Ligand Library

We synthesized a small library of stereochemically well-defined aziridines bearing tunable sulfonyl and sulfinyl warhead activating groups surrounding a conserved spirocyclic oxindole core—a privileged motif in drug discovery (Figure 1a).^[32–37] Although oxindole-based sulfonyl aziridines have been shown to react with indoles, thiols, alcohols, and amines in a flask, their utility and limitations (toxicity, GSH stability, etc.) are unexplored in cellular, proteome-wide contexts as required for covalent drug discovery.^[38,39] This fact, together with the observation that their sulfinyl congeners are even less interrogated in similar contexts, prompted us to synthesize and interrogate these novel chiral probes in a cellular setting with the knowledge that aziridines and related azirines are recognized electrophiles with a range of reactivities toward numerous amino acid side-chains.^[38–41]

We screened this bespoke covalent library in HEK293 cells expressing a HiBiT tag on the endogenous loci of MYC to identify molecules that lowered HiBiT-MYC levels (Figure 1b). From an initial small library screen, we were pleased to identify several molecules that significantly lowered HiBiT-MYC levels by >50%—KL2-236, KL2-230, KL4-018, KL3-284, KL2-168, and KL2-194 (Figure 1b). Although substituents appended to the oxindole ring generally decreased activity (i.e., KLE-017/KLE-018, KLE-015/KLE-016, KLE-112A/KLE-112B, KLE-113A/KLE-113B), initial modifications to the oxindole nitrogen were tolerated (see KL3-284). Interestingly, enantiomeric sulfonyl aziridine-containing compounds, KL2-194 and KL2-168, showed only modest differences in their ability to attenuate HiBiT-MYC levels and were also significantly cytotoxic, thus limiting their further use (Figure 1b, Figure S1a). In contrast, however, KL2-236, which possessed a sulfinyl activating group of attenuated reactivity, showed interesting patterns of stereoselective and dose-responsive HiBiT-MYC loss compared to its three stereoisomers (Figure 1c). Although KL2-236 is the most active stereoisomer in the series, its enantiomer KL2-230 also showed comparable activity. A diastereomer of these compounds, KL4-018, showed attenuated activity; however, its enantiomer, KL4-019, was largely inactive. This pattern of stereoselective activity also held for oxindoles KL3-284 and KL3-281, KLE-112A and KLE-112B, and KLE-113A and KLE-113B. None of the other compounds screened, including the four stereoisomers KL2-236, KL2-230, KL4-018, or KL4-019, showed more than 25% impairment in cell viability (Figure S1a).

We next tested the chemoselectivity of the four sulfinyl aziridine stereoisomers alongside the sulfonyl aziridine KL2-194 with an artificial peptide bearing 15 of the 20 amino

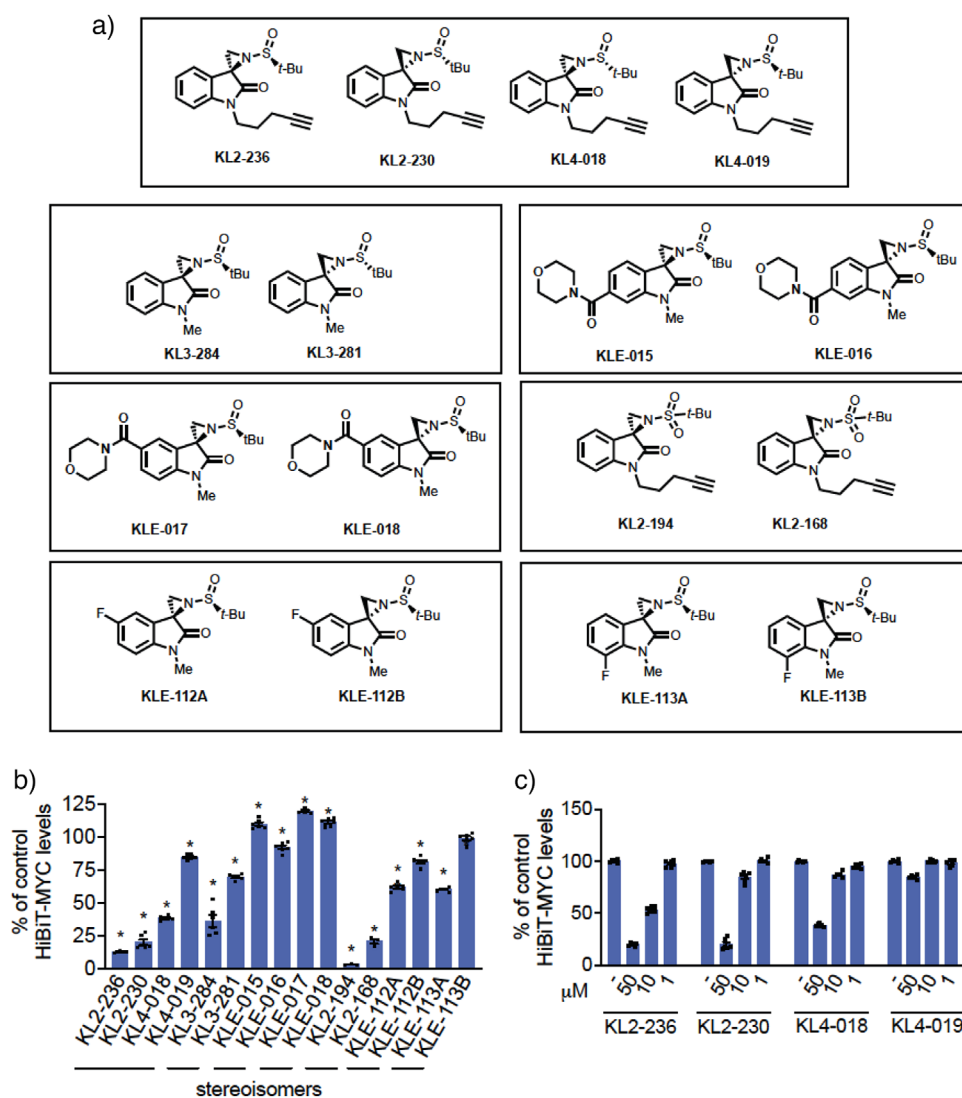


Figure 1. Screening a covalent ligand library for stereoselective MYC degradation. a) Structures of members of a stereochemically-defined sulfanyl or sulfonyl oxindole aziridine covalent ligand library. b) HiBiT-MYC HEK293-LgBiT cellular screen for MYC degraders. HiBiT-MYC HEK293-LgBiT cells were treated with DMSO vehicle or covalent compound (50 μM) for 24 h, and MYC levels were detected with the Nano-Glo HiBiT Lytic Detection System. c) Dose-response of KL2-236 and its isomers in HiBiT-MYC cells. HiBiT-MYC HEK293-LgBiT cells were treated with DMSO vehicle, KL2-236, KL2-230, KL4-018, or KL4-019 for 24 h, and MYC levels were detected with the Nano-Glo HiBiT Lytic Detection System. Data in (b,c) are presented as individual replicate values and average \pm sem percent of DMSO vehicle-treated controls. Significance is expressed as $*p < 0.05$ compared to DMSO vehicle-treated controls.

acids, including most nucleophilic amino acids, to assess amino acid reactivity preferences. We found that these compounds only reacted with cysteine and not with any other nucleophilic amino acid, including glutamic/aspartic acids, serines, tyrosines, threonines, lysines, or methionines in this experiment (Figure S1b). As expected, KL2-194, which possesses a more highly oxidized sulfur atom, was more reactive than the four stereoisomers KL2-236, KL2-230, KL4-018, and KL4-019 (Figure S1b,c). The higher reactivity of the sulfonyl aziridine KL2-194 compared to the sulfanyl aziridine counterparts is consistent with the higher degree of cytotoxicity observed with KL2-194. We also tested the in vitro stability of KL2-236 and KL4-019 in the presence of glutathione (GSH) and observed comparable GSH

half-lives of 50.6 min for KL2-236 and 59.4 min for KL4-019, respectively. These values are longer than previously reported in vitro GSH stability of clinically approved covalent drugs such as afatinib and neratinib with GSH half-lives of ~ 30 min.^[42] Overall, while our cellular data showed pronounced bioactivity differentiation between KL2-236 and its diastereomer KL4-019, these two compounds showed similar inherent reactivity with cysteine in a linear artificial peptide and with GSH. Moreover, our data also demonstrated that these sulfonyl aziridines were preferentially cysteine reactive, although we cannot rule out potential adducts that may form with other nucleophilic amino acids that may be reversible or unstable using traditional mass spectrometry approaches (Figure S1c).

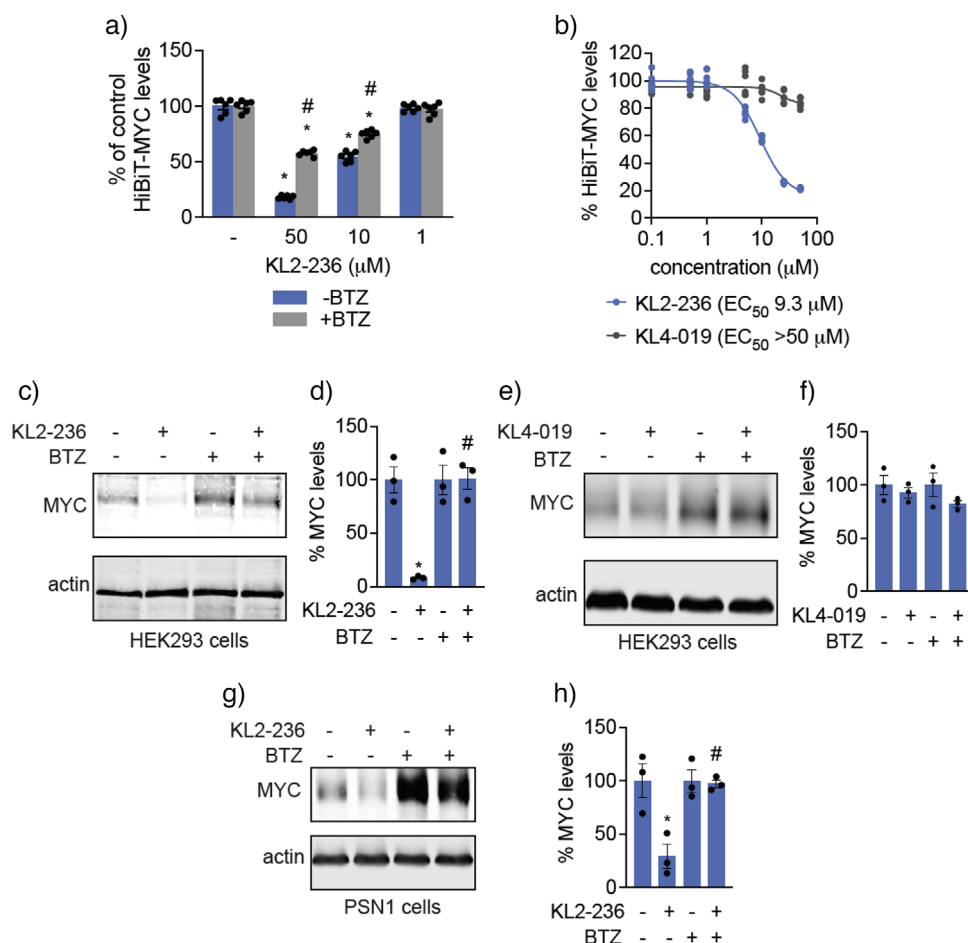


Figure 2. Characterization of KL2-236 and its stereoisomers. a) Proteasome dependence of HiBiT-MYC loss. HiBiT-MYC HEK293-LgBiT cells were pretreated with proteasome inhibitor bortezomib (500 nM) for 1 h before treatment of DMSO vehicle or KL2-236 for 24 h, and MYC levels were detected by luminescence. b) Dose-response of HiBiT-MYC degradation. HiBiT-MYC HEK293-LgBiT cells were treated with DMSO vehicle, KL2-236, or KL4-019 for 24 h, and MYC levels were detected by luminescence. c–f) MYC degradation in HEK293 cells. HEK293 cells were treated with DMSO vehicle or bortezomib (500 nM) for 1 h before treatment of DMSO vehicle or KL2-236 c,d) or KL4-019 (50 μM) e,f) for 24 h and MYC and loading control actin levels were assessed by Western blotting c,e) and quantified d,f). g,h) MYC degradation in PSN1 pancreatic cancer cells. PSN1 cells were treated with DMSO vehicle or bortezomib (500 nM) for 1 h before treatment with DMSO vehicle or KL2-236 for 2 h, and MYC and loading control actin levels were assessed by Western blotting g) and quantified h). Blots in (c,e) represent $n = 3$ biologically independent replicates per group. Bar graphs in (a,d,f,h) show individual replicate values and average \pm sem. Significance in (a,d,f,h) is shown as * $p < 0.05$ compared to vehicle-treated controls and # $p < 0.05$ compared to the respective KL2-236-treated groups.

Given that oxindole KL2-236 showed the best activity in reducing MYC without deleterious cytotoxicity and possessed a diastereomeric negative control compound (KL4-019), we prioritized downstream biological studies using this molecule. Confirming that HiBiT-MYC loss was through proteasome-mediated degradation rather than transcriptional downregulation, we observed significant attenuation of KL2-236-mediated HiBiT-MYC loss upon pretreatment of cells with the proteasome inhibitor bortezomib (Figure 2a). We also demonstrated dose-responsive loss of HiBiT-MYC with KL2-236, but not with KL4-019, with an 50% effective concentration (EC₅₀) value of 9.3 and >50 μM, respectively (Figure 2b). We further confirmed the proteasome-dependent degradation of endogenous MYC with KL2-236, but not with inactive stereoisomer KL4-019, in wild-type HEK293 cells (Figure 2c–f). We also demonstrated proteasome-mediated loss of MYC with KL2-236 treatment in more

cancer-relevant PSN-1 pancreatic cancer cells with MYC amplification (Figure 2g,h).^[43] We also synthesized unreactive analogs of KL2-236, including four stereoisomeric pairs of reduced, ring-opened analogs lacking an aziridine as well as analogs possessing an oxazolidinone instead of the sulfinyl aziridine warhead (Figure S2). None of these unreactive analogs degraded HiBiT-MYC, suggesting the importance of covalency in the degradation of MYC (Figure S2).

Characterizing KL2-236 Interactions with MYC

We next sought to determine whether KL2-236 directly interacted with MYC in vitro or in cancer cells. Given that KL2-236 had an alkyne handle for directly conjugating analytical handles through copper-catalyzed azide-alkyne cycloaddition (CuAAC), we exploited this feature to characterize its

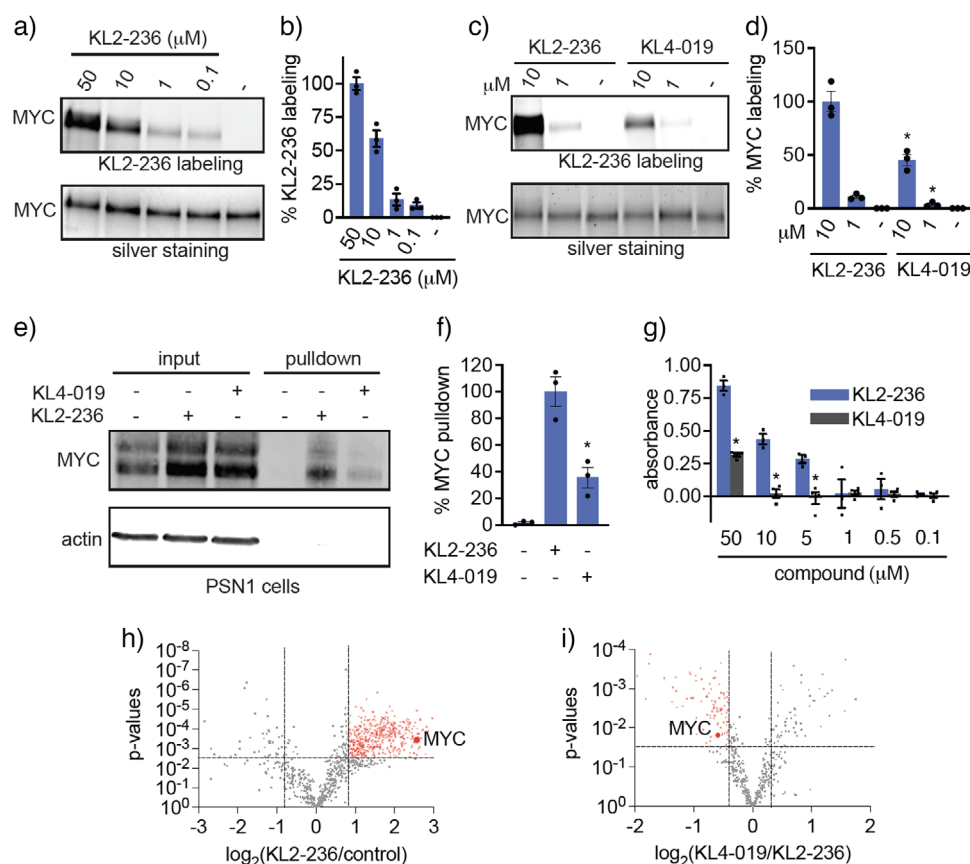


Figure 3. Characterization of KL2-236 Interactions with MYC. a–d) Gel-based ABPP of KL2-236 and KL4-019 with pure human MYC/MAX protein. Pure MYC/MAX human protein complex was treated with DMSO vehicle, KL2-236, or KL4-019 for 1 h, after which probe-modified protein was subjected to CuAAC with an azide-conjugated rhodamine, separated by SDS/PAGE and visualized by in-gel fluorescence (a,c) and quantified (b,d). Gels were silver stained to account for MYC protein loading. e,f) KL2-236 versus KL4-019 engagement of MYC in PSN1 cells. PSN1 cells were pretreated with BTZ (500 nM) for 1 h before treatment with DMSO vehicle, KL2-236 (50 μ M) or KL4-019 (50 μ M) for 2 h, after which probe-modified proteins were subjected to CuAAC with an azide-functionalized biotin, after which probe-modified proteins were enriched with avidin beads, eluted, and input and pull-down eluate was separated by SDS/PAGE and MYC and negative control protein actin were detected by Western blotting (e) and quantified (f). g) ELISA-ABPP assessment of KL2-236 versus KL4-019 cellular engagement of MYC in DLD-1 MYC-HiBiT expressing cells. DLD-1 MYC-HiBiT expressing cells were treated with DMSO vehicle, KL2-236, or KL4-019 for 1 h after which probe-modified proteins were appended with a biotin handle by CuAAC, and HiBiT-MYC was captured and immobilized on plate using a HiBiT antibody and then compound-engaged HiBiT-MYC was detected by streptavidin HRP. h,i) KL2-236 versus DMSO (h) or KL2-236 versus KL4-019 (i) chemoproteomic profiling in PSN1 cells. PSN1 cells were pretreated with BTZ (500 nM) for 1 h before treatment with DMSO vehicle, KL2-236 (50 μ M) or KL4-019 (50 μ M) for 2 h, after which probe-modified proteins were subjected to CuAAC with an azide-functionalized biotin, after which probe-modified proteins were enriched with avidin beads, eluted, and input and pull-down eluate was tryptically digested and analyzed and quantified by LC-MS/MS. Gels, blots, and data in (a–i) represent $n = 3–4$ biologically independent replicates per group. Data for (h,i) can be found in Tables S1 and S2.

interactions using ABPP-based approaches. We first demonstrated direct covalent labeling of pure human full-length MYC in the MYC/MAX protein complex in a dose-responsive manner, visualized through CuAAC-mediated conjugation of a rhodamine fluorophore and gel-based ABPP (Figure 3a,b). Strikingly, stereoselective labeling was also observed between KL2-236 and KL4-019, even at this pure MYC/MAX protein complex level (Figure 3c,d). We also demonstrated direct covalent binding to pure MYC without MAX as well (Figure S3a). We did not observe any labeling of MAX.

To understand where our molecule was binding to MYC, we assessed the KL2-236 modification site in the MYC/MAX pure protein complex through mass spectrometry (MS) analysis of KL2-236-modified MYC pepsin digests. The only

modification found was on cysteine C203 (Figure S3b,c). These data showed direct and covalent binding of KL2-236 to MYC in vitro.

We next assessed direct MYC target engagement in living cells. Treating PSN-1 cells with KL2-236, appending a biotin enrichment handle through CuAAC under denaturing conditions, and avidin-enriching KL2-236-modified proteins, we observed significant and stereoselective MYC enrichment with KL2-236 treatment over both the less active diastereomer KL4-019 and vehicle-treated controls (Figure 3e,f). Using an orthogonal enzyme-linked immunosorbent assay (ELISA)-ABPP approach wherein we treated HiBiT-MYC expressing DLD-1 cells with KL2-236 or KL4-019, appended a biotin handle by CuAAC under denaturing conditions, captured and immobilized HiBiT-MYC using a HiBiT

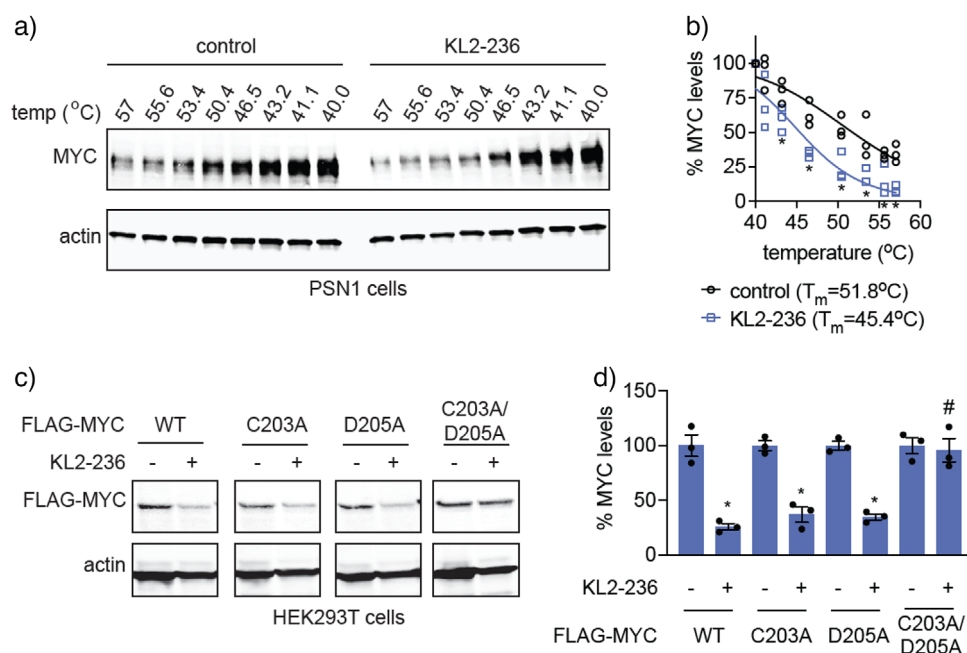


Figure 4. Understanding the mechanism through which KL2-236 degrades MYC. a,b) Cellular thermal shift assay (CETSA) of KL2-236 on MYC and negative control actin in PSN1 cells. PSN1 cells were treated with DMSO vehicle or KL2-236 (50 μ M) for 4 h. Cells were then heated at the designated temperatures, cells were harvested and lysed, insoluble proteins were pelleted, and soluble proteins were separated by SDS/PAGE and MYC and negative control actin levels were detected by western blotting a) and quantified b). c,d) FLAG-MYC degradation with KL2-236 treatment. HEK293T cells stably expressing FLAG-MYC wild-type (WT), C203A, D205A, or C203A/D205A were treated with DMSO vehicle or KL2-236 (50 μ M) for 24 h after which proteins were separated by SDS/PAGE and FLAG-MYC and loading control actin were detected c) and quantified d) by Western blotting. Blots in (a,c) represent $n = 3$ biologically independent replicates per group. Data in (b) shows individual replicate values. Data in (d) shows individual replicate and average \pm sem values. Significance in (b,d) expressed * $p < 0.05$ compared to vehicle-treated controls and # $p < 0.05$ compared to KL2-236 treated FLAG-MYC WT control groups in (d).

antibody, and reading out compound-engaged HiBiT-MYC by streptavidin-HRP, we also observed dose-responsive and significant stereoselective KL2-236 engagement of MYC-HiBiT over KL4-019 (Figure 3g,d). Through quantitative chemoproteomic profiling of KL2-236-enriched targets, we identified 437 proteins enriched by $\log_2 > 0.8$ with $p < 0.003$, including MYC out of 1048 proteins quantified (Figure 3h, Table S1). MYC and 101 other proteins were also enriched by KL2-236 more significantly than KL4-019 (Figure 3i, Table S2). Among these off-targets that were stereoselectively engaged were highly abundant enzymes that bear a catalytic and hyper-reactive cysteine, such as glyceraldehyde-3-phosphate dehydrogenase (GAPDH) (Table S2).^[44] To confirm that GAPDH was indeed an off-target that was stereoselectively and functionally engaged by KL2-236, and not non-specific capture, we showed that GAPDH was inhibited by KL2-236, more so than KL4-019 (Figure S4). Interestingly, the stereoselectivity of GAPDH inhibition differed from that of MYC, showing less GAPDH inhibition with KL2-230 and KL4-019, compared to KL2-236 and KL4-018 (Figure S4). Although these data showed that KL2-236 had several hundred off-targets and relatively poor selectivity, they also demonstrated direct stereoselective engagement of MYC with KL2-236 over its isomer, KL4-019, in cells. Given the significant challenges faced in directly targeting MYC, we were still intrigued by the stereoselective engagement of MYC observed in living cells.

To further demonstrate MYC engagement in cells by KL2-236, we performed a cellular thermal shift assay (CETSA) in PSN1 cells. Instead of observing the stabilization of MYC thermal stability, we found a significant destabilization of MYC thermal stability with KL2-236 treatment in PSN1 cells with a 6.4 $^{\circ}$ C shift in the temperature at which 50% of MYC was stable (T_m) from 51.8 $^{\circ}$ C to 45.4 $^{\circ}$ C (Figure 4a,b). This destabilization of MYC by KL2-236 was reminiscent of our previously discovered covalent destabilizing MYC degrader EN4 and our destabilizing CTNNB1 degrader NF764, indicating that KL2-236 was degrading MYC through a similar destabilizing degradation mechanism compared to traditional PROTACs and molecular glue degraders.^[21,22,45,46]

To assess whether KL2-236 engagement of C203 was responsible for MYC degradation, we determined whether mutagenesis of C203 to alanine would attenuate MYC loss. Disappointingly, KL2-236 still degraded MYC C203A to the same extent as the wild-type protein in HEK293T cells (Figure 4c,d). We next sought to address whether there might be neighboring residues proximal to C203 that KL2-236 could react with in the absence of C203 or residues that may coordinate the reactivity of C203. We performed mass spectrometry-based activity-based protein profiling (MS-ABPP) with KL2-236 as a probe to understand its site-specific and sequence-specific reactivity in complex PSN1 proteomes (Figure S5a–c, Table S3). Unfortunately, we were unable to capture the KL2-236 modified tryptic MYC

peptide, likely due to the long length of the C203-bearing tryptic peptide and the relatively low abundance of MYC. However, we successfully captured several hundred KL2-236-modified peptides from complex proteomes of other proteins (Table S3). By using an unbiased approach to determine the amino acid labeling preferences of KL2-236, we still observed a high chemoselectivity for cysteine over any other amino acid (Figure S5a, Table S3). When we performed sequence preference analysis of neighboring residues to the KL2-236-modified cysteines, we found a preference for acidic residues such as aspartic or glutamic acid either -1 or +2 from the modified cysteine (Figure S5b, Table S3). Upon analyzing a previously published chemoproteomic profiling dataset using a broadly reactive alkyne-functionalized iodoacetamide (IA-alkyne) probe,^[47] we did not observe this preference (Figure S5c, Table S3). Indeed, C203 is also flanked by E202 and D205. We were unable to identify E202 or D205 modifications with KL2-236, but we conjectured that these adducts may be potentially reversible. Interestingly, upon modeling this region in MYC with AlphaFold,^[48,49] while the region where C203 resides is generally disordered, there is relatively higher confidence around D205, where D205 is hydrogen-bonded with a neighboring S207 in a helix (Figure S6). We fully recognize that AlphaFold trains its model on existing structures and that all MYC-containing entries include MAX and may thus bias predictions of MYC structure toward helical structure. We also acknowledge that structural insights into this largely disordered region of MYC are purely speculative. Nonetheless, we postulated that one of these acidic residues, particularly D205, could activate the C203 thiol, making it more nucleophilic and hyper-reactive, and that KL2-236 could also potentially react with one of these acidic residues in the absence of C203. Alternatively, one of these acidic residues could be required for protonation of the chiral sulfoxide and subsequent positioning of the electrophile for covalent bond formation. Also, another possibility was that in the absence of C203, KL2-236 may be able to react with E202 or D205.

Mutagenesis of E202 or D205 alone also did not attenuate MYC degradation from KL2-236 treatment (Figure 4c,d, Figure S7a,b). However, we observed complete attenuation of MYC degradation with the MYC D205A/C203A double mutant (Figure 4c,d). We did not observe this rescue with the MYC E202A/C203A mutant (Figure S7a,b). Overall, our results suggest that in addition to C203, D205 is involved in the reactivity and activity of KL2-236 with MYC. Thus, while KL2-236 is a pathfinder molecule, we have demonstrated that the observed degradation of MYC is mediated through on-target activity, resulting from direct engagement of MYC.

Impact of KL2-236 on MYC Transcriptional Activity

Thus far, we have shown that KL2-236 stereoselectively engages MYC in vitro and in cells at C203, potentially involving D205, to destabilize and degrade MYC in a proteasome-dependent manner. We next wanted to understand whether KL2-236 impairs MYC transcriptional activity

and downregulates MYC target genes in cancer cells. KL2-236, but not the inactive isomer KL4-019, dose-responsively inhibited MYC luciferase reporter transcriptional activity in HEK293T cells with an EC₅₀ of 4.5 μM versus >50 μM, respectively (Figure 5a). KL2-236 treatment in PSN1 cancer cells significantly modulated >280 transcript levels (Figure 5b, Table S4). Consistent with KL2-236 action on inhibiting and degrading MYC, gene set enrichment analysis (GSEA) of significantly modulated genes revealed the most significant pathway affected with the lowest normalized enrichment score as MYC targets, followed by IFNα response, E2F targets, oxidative phosphorylation, and IFNγ response (Figure 5c,d, Figure S7c, Table S4). In contrast, while MYC target genes do tend to be at the end of the ranks in MYC target gene enrichment plots, they are not significantly repressed in GSEA testing against randomized permutations (Figure S7c, Table S4). Although MYC target genes are enriched in the top and bottom five enriched pathways, it is not the most significantly enriched pathway, and MYC target genes show much less statistical significance compared to what is observed with KL2-236 (Figure S7c,d, Table S4). Overall, while the global transcriptomic comparison of KL2-236 and KL4-019 compared to DMSO vehicle-treated controls does not show absolute stereoselective effects, MYC target genes are more significantly enriched with KL2-236 compared with KL4-019 treatment in GSEA. This is consistent with our pure protein and intracellular MYC engagement data comparing KL2-236 to KL4-019, showing that both compounds engage MYC, but KL2-236 labels and engages MYC to a higher degree compared to KL4-019 (Figure 3c-i). Our data collectively demonstrated that KL2-236 engages and degrades MYC, inhibits MYC transcriptional activity, and downregulates MYC target genes in cells.

Improving the Durability of MYC Degradation

While we showed compelling results with KL2-236 of a covalent molecule that stereoselectively engages MYC directly in cells to destabilize, degrade, and inhibit MYC, KL2-236 only shows acute loss of MYC in the first 2–6 h of treatment with recovery of MYC protein levels by 12 h in PSN1 cancer cells where MYC turnover is rapid (Figure S8a,b). Indeed, this feature of MYC (rapid turnover) presents a known challenge for small molecule drug discovery efforts.^[50] In addition, KL2-236 had many off-targets at concentrations required for MYC degradation. Thus, we sought to develop a more potent, selective, and durable MYC degrader. The reaction of spirocyclic oxindole sulfonyl aziridines with nucleophiles is proposed to involve in situ aziridinium ion formation generated using the oxindole nitrogen.^[38,39] As such, we suspected that substituents on nitrogen would be important in modulating the protein reactivity of these sulfinyl aziridines as well. We generated analogs with various alterations to this site and assessed structure-activity relationships in degrading HiBiT-MYC in cells, assessing both the EC₅₀ potency of degradation and the maximal percent degradation (*D*_{max}) (Figure 6a,b). As expected, groups that remove electron density from the oxindole nitrogen (see: KLE-142, KLE-144, and

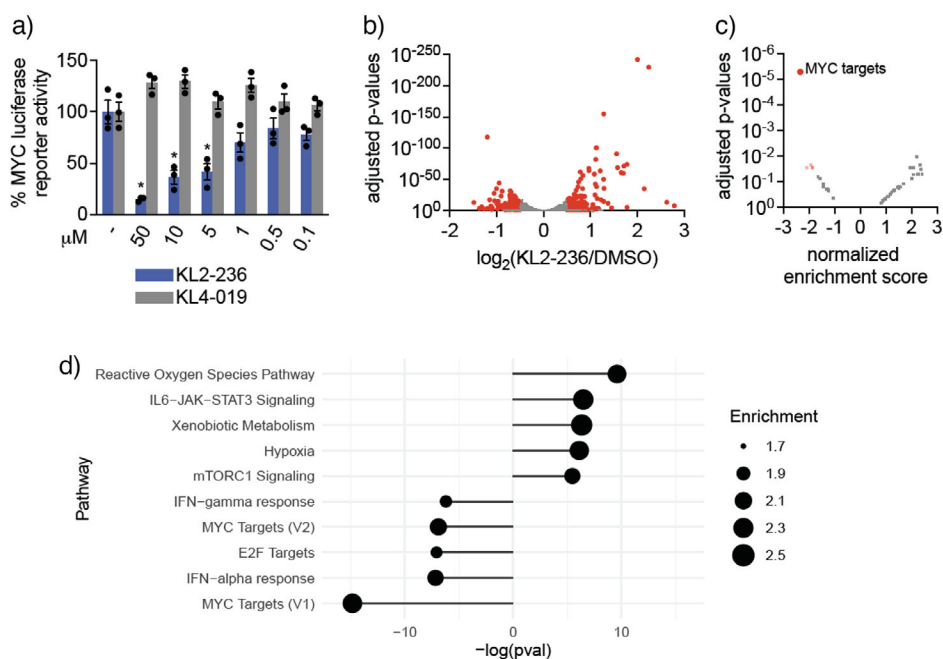


Figure 5. Functional effects of KL2-236 on MYC transcriptional activity. a) MYC luciferase reporter transcriptional activity in HEK293T cells. HEK293T cells expressing an MYC luciferase reporter were treated with DMSO vehicle, KL2-236, or KL4-019 for 24 h, after which MYC transcriptional activity was read out by luminescence. b) RNA sequencing of KL2-236 in PSN1 cells. PSN1 cells were treated with DMSO vehicle or KL2-236 (50 μM) for 2 h. Resulting RNA from treated cells were sequenced and quantified. Shown in red are significantly altered transcripts ($p < 0.05$, $< \log_2 -0.5$ or $> \log_2 0.5$). Data are in Table S4. c,d) Gene enrichment analysis shows significantly altered pathways and normalized enrichment scores, detailed in Table S4. These plots highlight the directionality, significance, and amount of enrichment of the top- and bottom- five pathways. “Enrichment” represents the Normalized Enrichment Score. Data in a–d) are from $n = 3$ biologically independent replicates per group. Data in (a) shows individual replicate and average \pm sem values. Significance in (a) expressed $*p < 0.05$ compared to vehicle-treated controls.

KLE-138) were largely inactive, as was the free N-H oxindole compound KL6-030. Likewise, a highly potent compound was achieved through attachment of an electron-rich *para*-anisole ring (see: KL4-219A). The *ortho*-anisole isomer (KL6-019A), which is twisted out of planarity and displays atropisomerism, was less active. Compound KL5-289A, which lacks the phenyl ring found in KL4-219A (and instead possesses a direct N-OMe linkage), also showed dampened activity as did related ethers KLE-217A and alkyne probe KL6-085A. These findings suggest that steric and/or physicochemical properties are important parameters in addition to electronic effects.

Gratifyingly, we found that KL4-219A showed more potent and durable degradation of MYC with an EC₅₀ of 1.7 μM and continued MYC loss after 24 h of treatment in PSN1 cells without showing any cytotoxicity (Figures 6a,b and 7a–d, Figures S8c and S9a,b). Like KL2-236, we also observed diminished HiBiT-MYC degradation and inhibition of MYC transcriptional reporter activity with the diastereomeric compound KL4-219B, compared to KL4-219A (Figure 7a,b,e). KL4-219A showed an EC₅₀ of 0.93 μM for inhibition of MYC transcriptional activity, compared to >50 μM with KL4-219B (Figure 7e). Similar to KL2-236, KL4-219A also significantly destabilized MYC in thermal shift assays (Figure 7f,g). The loss of MYC conferred by KL4-219A was attenuated upon pretreatment of cells with a proteasome inhibitor, confirming proteasome dependence of MYC loss, whereas no MYC degradation was observed with KL4-219B treatment (Figure

S9c–f). Confirming a similar mechanism of action as KL2-236, we showed that MYC degradation was still observed in wild-type and single mutants C203A or D205A, but was completely attenuated in C203A and D205A-double mutant MYC-expressing cells (Figure 8a,b).

Interestingly, these analogs, which induced more long-lasting degradation, had shorter in vitro GSH half-lives (19.3 and 26.3 min for KL4-219A and KL4-219B, respectively) as compared to KL2-236 and KL4-019. Thus, the sustained MYC degradation observed with KL4-219A may be related to the kinetics of degradation or other physicochemical parameters (such as permeability and potency) rather than warhead stability. We further showed that analogs of KL4-219A and KL4-219B that lack a reactive warhead—KL6-278A and KL6-278B, respectively—did not degrade MYC (Figure S10a,b). Previous studies have suggested that electrophiles may cause cell stress and induce the formation of stress granules, which could complicate the interpretation of protein degradation.^[51] We found that neither KL2-236 nor KL4-219A causes stress granule formation at concentrations used in this study compared to the positive control sodium arsenite (Figure S11).

Given that our original hit compound KL2-236 showed hundreds of off-targets, we sought to assess whether KL4-219A was more selective. First, we performed global quantitative proteomic profiling to assess the selectivity of MYC degradation. We were pleased to see that KL4-219A showed highly selective degradation of MYC with only three other

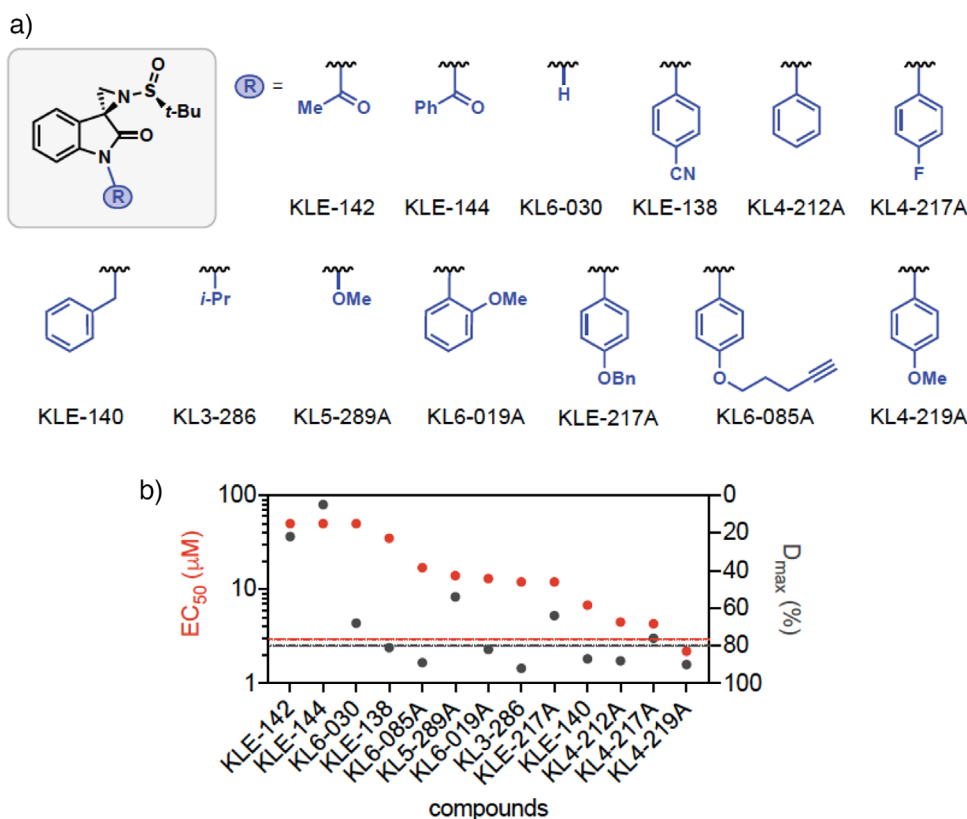


Figure 6. Structure–activity relationship of sulfanyl aziridines. a) Analogs of KL2-236. b) HiBiT-MYC HEK293-LgBiT cells were pretreated DMSO vehicle or compound in dose-response experiments for 24 h, and HiBiT-MYC levels were detected by luminescence. D_{\max} and EC_{50} of degradation were calculated and plotted. Data are from $n = 3$ biologically independent replicates/group.

proteins that were significantly lowered—MCL1, CDCA4, and ID1 (Figure 8c, Table S5). Interestingly, MCL1 has been shown to be a direct MYC target gene.^[52] Second, chemoproteomic profiling of KL4-219A-outcompeted proteins from KL2-236 enrichment showed significant out-competition of MYC; among >968 proteins quantified, only 65 other proteins were significantly outcompeted by KL4-219A pretreatment (Figure 8d, Table S6). We also tested alkyne-functionalized analogs of KL4-219A and KL4-219B—KL6-085A and KL6-085B, respectively (Figure 8e). These probes showed stereoselective degradation of HiBiT-MYC, albeit with attenuated potencies (Figure 8f). Chemoproteomic profiling with KL6-085A showed significant MYC enrichment compared to vehicle-treated controls, with 98 other off-targets, considerably less than the >400 off-targets observed with KL2-236 (Figure 8g, Table S7). Comparative chemoproteomic profiling between KL6-085B and KL6-085A showed significant stereoselective engagement of MYC, with only 56 other off-targets showing stereoselective engagement, compared to >100 off-targets comparing KL4-019 and KL2-236 (Figure 8h, Table S8). Overall, we developed an improved stereoselective MYC degrader, KL4-219A. Although this molecule still possesses several off-targets, it shows improved potency and selectivity to our original hit molecule, and is an important pathfinder molecule for future optimization studies.

Discussion

Our findings address a longstanding challenge in chemical biology and oncology by demonstrating that MYC, a notoriously “undruggable” oncogenic transcription factor with extensive intrinsic disorder, can indeed be directly and stereoselectively targeted. Through a focused covalent library of stereochemically defined electrophiles, we discovered the hit compound KL2-236, which engages MYC at C203 with contribution from the neighboring D205 with distinct selectivity to its isomers to trigger proteasome-mediated degradation of MYC. Although the nature of the interactions between these small molecules and MYC remains unclear at the molecular level, this study further highlights the power of chiral, covalent molecules to interrogate structurally undefined proteins. We also introduce the sulfanyl aziridine as a robust, protein-reactive electrophilic warhead with desirable stability, modulable reactivity, and opportunities for direct at-warhead stereochemical tuning. The engagement of KL2-236 relative to KL4-019, even at the pure protein complex level, also further underscores the importance of expanding stereochemical space in covalent warhead design for targeting intrinsically disordered protein regions beyond that of just enantiomers, as a greater number of stereocenters may be required for observable compound differentiation.^[18,23] Spirocyclic oxindole sulfanyl aziridines react with nucleophiles under mild

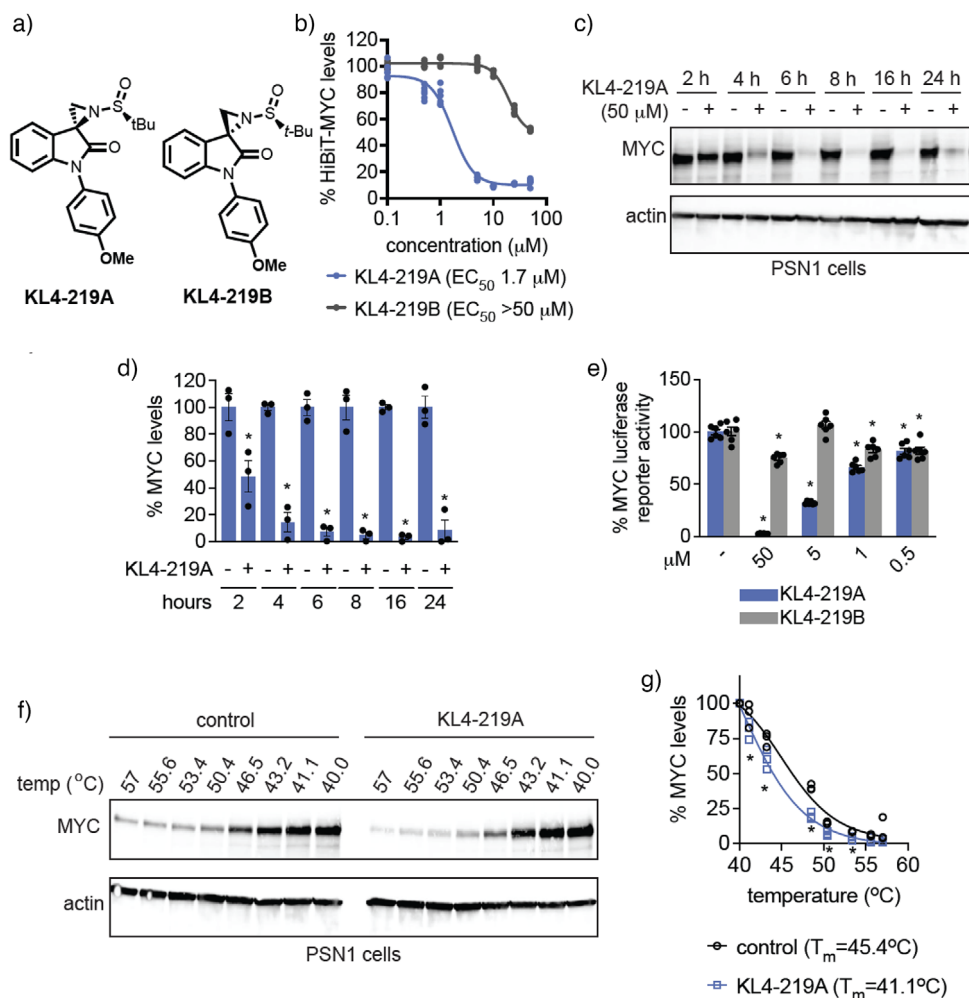


Figure 7. More Durable Analog of KL2-236: KL4-219A. a) Structure of KL4-219A and diastereomer KL4-219B. b) HiBiT-MYC HEK293-LgBiT cell dose-response with KL4-219A/B. HiBiT-MYC HEK293-LgBiT cells were treated with DMSO vehicle, KL4-219A, or KL4-219B for 24 h, and MYC levels were detected with the Nano-Glo HiBiT Lytic Detection System. c,d) Time-course of KL4-219A-mediated MYC degradation in PSN1 cells. PSN1 cells were treated with a DMSO vehicle or KL4-219A (50 μM) at designated times, and MYC and loading control actin levels were assessed by Western blotting c) and quantified d). e) MYC luciferase reporter transcriptional activity in HEK293T cells. HEK293T cells expressing a MYC luciferase reporter were treated with DMSO vehicle, KL4-219A, KL4-219B for 24 h, after which MYC transcriptional activity was read out by luminescence. f,g) CETSA of KL4-219A on MYC and negative control actin in PSN1 cells. PSN1 cells were treated with DMSO vehicle or KL4-219A (50 μM) for 4 h. Cells were then heated at the designated temperatures, cells were harvested and lysed, insoluble proteins were pelleted, and soluble proteins were separated by SDS/PAGE and MYC and negative control actin levels were detected by Western blotting f) and quantified g). Data or blots in (b–g) represent $n = 3$ –6 biologically independent replicates per group. The blots are representative. The bar and line graphs in (b,d,e,g) show individual replicate values and average \pm sem for bar graphs and average for line. Significance is shown as $*p < 0.05$ compared to vehicle-treated controls for each group.

aqueous conditions owing to hydrogen-bond activation of the sulfonyl group with water.^[38,39] This could suggest context-specific, two-point activation for the even less reactive sulfinyl aziridines reported herein, whereby acidic protein residues position or activate the chiral sulfoxide before covalent bond formation occurs. Such a mechanism would be sensitive to local chiral environments found in dynamic structures within intrinsically disordered regions, in accordance with our stereochemical findings. Alternatively, sulfinyl aziridines may react with aspartic or glutamic acids in certain contexts as well, but these adducts might be reversible or unstable and thus difficult to detect with typical proteomics methods.

Because MYC is a central driver of growth and metabolism in various cancers, even modest decreases in MYC protein levels can have broad anticancer effects. By mapping the binding sites and confirming their importance in MYC degradation through mutagenesis studies, we uncovered a cooperative role for C203 and D205 in KL2-236-mediated MYC degradation, suggesting that residue adjacency and local electrostatics can significantly influence small-molecule reactivity within disordered protein regions. Consistent with this mechanism, KL2-236 not only degraded MYC but also demonstrably reduced its transcriptional activity—underscoring the central role of

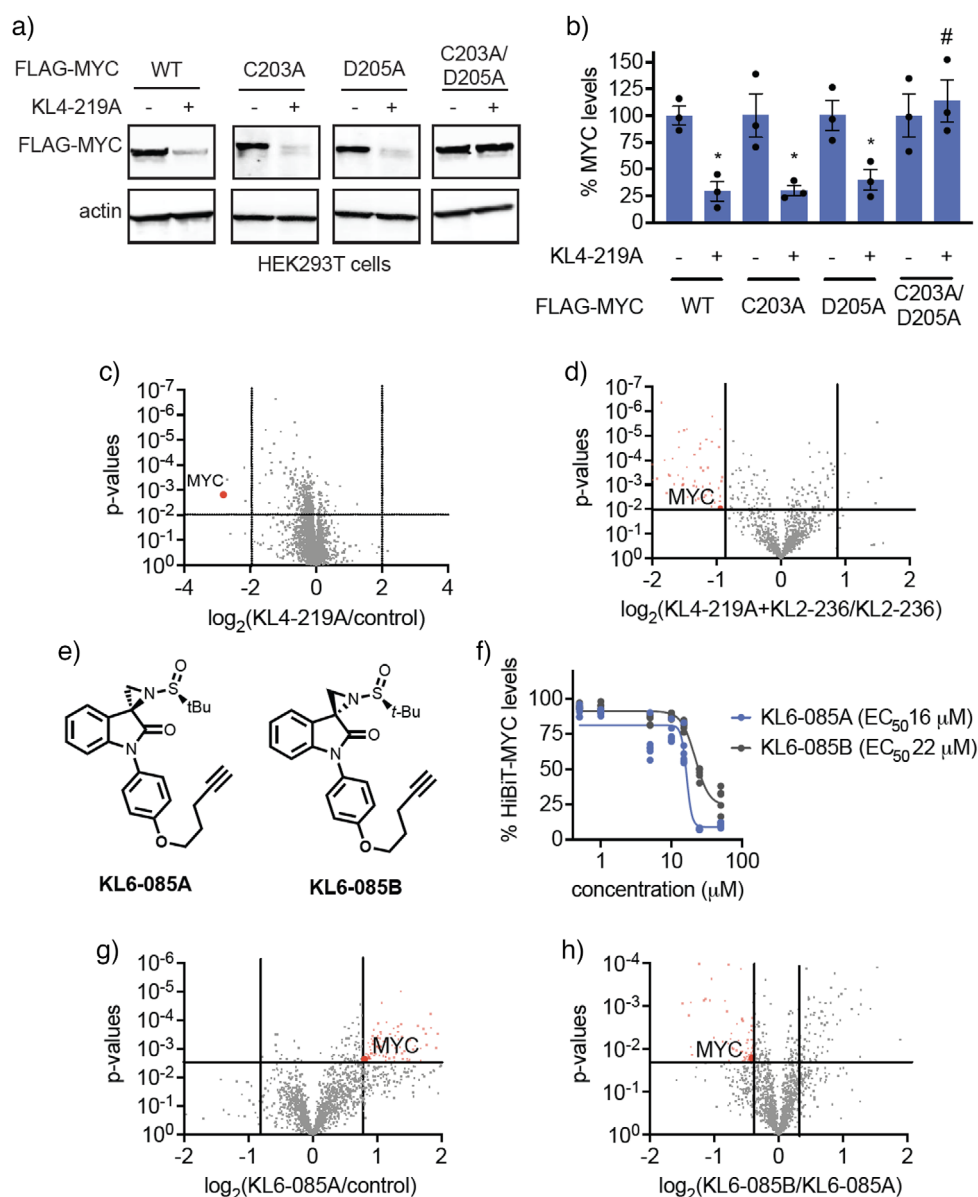


Figure 8. Characterization of KL4-219A. a,b) FLAG-MYC degradation with KL4-219A treatment. HEK293T cells stably expressing FLAG-MYC wild-type (WT), C203A, D205A, or C203A/D205A were treated with DMSO vehicle or KL4-219A (50 μM) for 24 h after which proteins were separated by SDS/PAGE and FLAG-MYC and loading control actin were detected a) and quantified b) by Western blotting. c) Quantitative proteomic profiling of KL4-219A in PSN1 cells. PSN1 cells were treated with DMSO vehicle or KL4-219A (50 μM) for 8 h. Protein level changes were assessed by TMT-based quantitative proteomic methods. Shown in red is MYC. d) Chemoproteomic profiling of KL4-219A. PSN1 cells were pretreated with proteasome inhibitor bortezomib (500 nM) for 30 min prior to treatment with DMSO vehicle or KL4-219A (100 μM) for 1 h and then treatment with KL2-236 (25 μM) for 4 h, after which resulting cell lysates were subjected to CuAAC mediated appendage of an azide-functionalized biotin handle, probe-modified proteins were enriched, tryptically digested, and analyzed by TMT-based quantitative proteomics. Shown in red are proteins that were significantly enriched and were outcompeted by KL4-219A. e) Structure of KL6-085A and diastereomer KL6-085B. f) HiBiT-MYC HEK293-LgBiT cell dose-response with KL6-085A/B. HiBiT-MYC HEK293-LgBiT cells were treated with DMSO vehicle, KL6-085A, or KL6-085B for 24 h, and MYC levels were detected with the Nano-Glo HiBiT Lytic Detection System. g,h) KL6-085A versus KL6-085B g) or KL6-085A versus KL6-085B h) chemoproteomic profiling in PSN1 cells. PSN1 cells were pretreated with BTZ (500 nM) for 1 h before treatment with DMSO vehicle, KL6-085A (50 μM) or KL6-085B (50 μM) for 2 h, after which probe-modified proteins were subjected to CuAAC with an azide-functionalized biotin, after which probe-modified proteins were enriched with avidin beads, eluted, and input and pulldown eluate was tryptically digested and analyzed and quantified by LC-MS/MS. Data for (c,d,g,h) are in Tables S5–S8. Data or blots in (a–d,f–h) represent $n = 3$ biologically independent replicates per group. The bar and line graphs in (b,f) show individual replicate values and average \pm sem values or average values, respectively, from $n = 3$ biologically independent replicates per group. Significance is shown as * $p < 0.05$ compared to vehicle-treated controls and # $p < 0.05$ compared to KL4-219A-treated FLAG-MYC wild-type cells.

structural destabilization in achieving functional inhibition of an intrinsically disordered transcription factor.

Moreover, we improved upon the liability of KL2-236 in only achieving acute and transient MYC degradation through the development of KL4-219A, which exhibits enhanced degradation durability. Furthermore, KL2-236 showed a high number of off-targets, whereas KL4-219A shows far fewer off-targets and shows exceptional selectivity for MYC degradation. Such iterative optimization exemplifies the power of rational medicinal chemistry approaches for improving the potency, selectivity, and temporal profile of covalent degraders. These differences in durability are likely driven by structural modifications that influence MYC engagement, covalent bond formation, proteasomal processing, and the stability and half-life of the molecule. Nonetheless, KL4-219A is still not of sufficient potency or selectivity and still requires further medicinal chemistry efforts for future translational applications. We can also not rule out potential confounding effects of these off-targets in the biological effects reported here for both KL2-236 and KL4-219A.

Another major question to be addressed in future work surrounds the mechanism by which MYC is degraded. We have not yet been able to identify an E3 ligase responsible for the observed proteasome-mediated degradation of MYC. We postulate that the destabilization may cause partial unfolding of MYC, either exposing a degron that is recognized by an E3 ligase or general quality control E3 ligases that recognize unfolded proteins. Future functional genomic screens to identify the mechanism of degradation of MYC, and more broadly these classes of destabilizing degraders, will be important for the future translatability of these molecules.

Further characterization of KL4-219A and more potent, selective, and metabolically stable analogs, particularly in physiologically relevant animal models, will be critical for translating these proof-of-concept findings into potential therapeutic interventions. Delineating how the surrounding protein environment in living systems affects compound reactivity and specificity will deepen our understanding of covalent ligand–protein interactions in intrinsically disordered regions. By demonstrating that intrinsically disordered proteins harbor exploitable cryptic sites, this work opens new vistas for targeting one of the most recalcitrant classes of oncogenic transcription factors.

Author Contributions

D.K.N., T.J.M., H.T.R., K.L. conceived of the project. H.T.R., K.L., C.S., E.L.L., B.C., S.M.B., F.J.G., D.C.B., S.H.H., D.D., D.K.N. performed experiments, analyzed data, and interpreted results. H.T.R., K.L., S.M.B., D.D., J.M.M., D.C.B., F.J.G., J.M.M., M.S., T.J.M., and D.K.N. wrote the paper.

Acknowledgements

The authors thank the members of the Nomura Research Group and Novartis BioMedical Research for critically reading the manuscript. This work was also supported by

Novartis Biomedical Research, the National Science Foundation Molecular Foundations for Biotechnology (MFB) grant (2127788), the UC Berkeley Molecular Therapeutics Initiative (MTI), Bakar Fellows Award, the Mark Foundation for Cancer Research ASPIRE Award, and the National Institutes of Health (R35CA263814, R01CA240981, UM1CA29410). The authors also thank Hasan, Lund, and the UC Berkeley NMR facility in the College of Chemistry (CoC-NMR) and Zhongrui at the QB3/chemistry mass spectrometry facility for spectroscopic assistance. Instruments in the College of Chemistry NMR facility are partly supported by NIH S10OD024998. K.L. acknowledges the National Science Foundation for a pre-doctoral graduate fellowship. RNA Sequencing was performed at the QB3 Genomics Facility at UC Berkeley, Berkeley, CA RRID :SCR_022170 and was supported by NIH S10 OD018174 Instrumentation Grant. The authors also recognize the RCNR Biological Imaging Facility at the University of California, Berkeley and Denise Schichnes for their microscopy facilities, expertise, and support.

Conflict of Interests

D.K.N. is a co-founder, shareholder, and scientific advisory board member for Frontier Medicines and Zenith. D.K.N. is also on the scientific advisory board of The Mark Foundation for Cancer Research, American Association for Cancer Research, Photys Therapeutics, Oerth Bio, Apertor Pharmaceuticals, Ten30 Biosciences, and Deciphera (a member of Ono Pharma). D.K.N. is also an Investment Advisory Partner for a16z Bio, an Advisory Board member for Droia Ventures, and an iPartner for The Column Group. S.M.B., D.D., F.J.G., J.M.M., D.C.B., M.S. are employees of Novartis.

Data Availability Statement

The data that support the findings of this study are available on request from the corresponding author. The data are not publicly available due to privacy or ethical restrictions.

Keywords: Activity-based protein profiling • Chemoproteomics • Covalent • Cysteine • MYC • Sulfinyl aziridine • Targeted protein degradation

- [1] M. J. Henley, A. N. Koehler, *Nat. Rev. Drug Discovery* **2021**, *20*, 669–688.
- [2] M. R. McKeown, J. E. Bradner, *Cold Spring Harb. Perspect. Med.* **2014**, *4*, a014266.
- [3] N. Meyer, L. Z. Penn, *Nat. Rev. Cancer* **2008**, *8*, 976–990.
- [4] H. Chen, H. Liu, G. Qing, *Signal Transduct. Target. Ther.* **2018**, *3*, 5.
- [5] T. R. Kress, A. Sabò, B. Amati, *Nat. Rev. Cancer* **2015**, *15*, 593–607.
- [6] C. V. Dang, E. P. Reddy, K. M. Shokat, L. Soucek, *Nat. Rev. Cancer* **2017**, *17*, 502–508.

- [7] J. R. Whitfield, M.-E. Beaulieu, L. Soucek, *Front. Cell Dev. Biol.* **2017**, *5*, 10.
- [8] C. M. Olson, B. Jiang, M. A. Erb, Y. Liang, Z. M. Doctor, Z. Zhang, T. Zhang, N. Kwiatkowski, M. Boukhali, J. L. Green, W. Haas, T. Nomanbhoy, E. S. Fischer, R. A. Young, J. E. Bradner, G. E. Winter, N. S. Gray, *Nat. Chem. Biol.* **2018**, *14*, 163–170.
- [9] N. B. Struntz, A. Chen, A. Deutzmann, R. M. Wilson, E. Stefan, H. L. Evans, M. A. Ramirez, T. Liang, F. Caballero, M. H. E. Wildschut, D. V. Neel, D. B. Freeman, M. S. Pop, M. McConkey, S. Muller, B. H. Curtin, H. Tseng, K. R. Frombach, V. L. Butty, S. S. Levine, C. Feau, S. Elmiligy, J. A. Hong, T. A. Lewis, A. Vetere, P. A. Clemons, S. E. Malstrom, B. L. Ebert, C. Y. Lin, D. W. Felsher, et al., *Cell Chem. Biol.* **2019**, *26*, 711–723.e14.
- [10] K. Mitchell, S. A. Sprowls, S. Arora, S. Shakya, D. J. Silver, C. M. Goins, L. Wallace, G. Roversi, R. E. Schafer, K. Kay, T. E. Miller, A. Lauko, J. Bassett, A. Kashyap, J. D'Amato Kass, E. E. Mulkearns-Hubert, S. Johnson, J. Alvarado, J. N. Rich, E. C. Holland, P. J. Paddison, A. P. Patel, S. R. Stauffer, C. G. Hubert, J. D. Lathia, *Genes Dev.* **2023**, *37*, 86–102.
- [11] J. Ding, G. Li, H. Liu, L. Liu, Y. Lin, J. Gao, G. Zhou, L. Shen, M. Zhao, Y. Yu, W. Guo, U. Hommel, J. Ottl, J. Blank, N. Aubin, Y. Wei, H. He, D. R. Sage, P. W. Atadja, E. Li, R. K. Jain, J. A. Tallarico, S. M. Canham, Y.-L. Chiang, H. Wang, *ACS Chem. Biol.* **2023**, *18*, 34–40.
- [12] C. T. Meyer, B. N. Smith, J. Wang, K. B. Teuscher, B. C. Grieb, G. C. Howard, A. J. Silver, S. L. Lorey, G. M. Stott, W. J. Moore, T. Lee, M. R. Savona, A. M. Weissmiller, Q. Liu, V. Quaranta, S. W. Fesik, W. P. Tansey, *Proc. Natl. Acad. Sci. USA* **2024**, *121*, e2408889121.
- [13] J. Ding, L. Liu, Y.-L. Chiang, M. Zhao, H. Liu, F. Yang, L. Shen, Y. Lin, H. Deng, J. Gao, D. R. Sage, L. West, L. A. Llamas, X. Hao, S. Kawatkar, E. Li, R. K. Jain, J. A. Tallarico, S. M. Canham, H. Wang, *J. Med. Chem.* **2023**, *66*, 8310–8323.
- [14] Y. Liu, M. P. Patricelli, B. F. Cravatt, *Proc. Natl. Acad. Sci. USA* **1999**, *96*, 14694–14699.
- [15] D. Kidd, Y. Liu, B. F. Cravatt, *Biochemistry* **2001**, *40*, 4005–4015.
- [16] E. Weerapana, C. Wang, G. M. Simon, F. Richter, S. Khare, M. B. D. Dillon, D. A. Bachovchin, K. Mowen, D. Baker, B. F. Cravatt, *Nature* **2010**, *468*, 790–795.
- [17] K. M. Backus, B. E. Correia, K. M. Lum, S. Forli, B. D. Horning, G. E. González-Páez, S. Chatterjee, B. R. Lanning, J. R. Teijaro, A. J. Olson, D. W. Wolan, B. F. Cravatt, *Nature* **2016**, *534*, 570–574.
- [18] E. V. Vinogradova, X. Zhang, D. Remillard, D. C. Lazar, R. M. Suci, Y. Wang, G. Bianco, Y. Yamashita, V. M. Crowley, M. A. Schafroth, M. Yokoyama, D. B. Konrad, K. M. Lum, G. M. Simon, E. K. Kemper, M. R. Lazear, S. Yin, M. M. Blewett, M. M. Dix, N. Nguyen, M. N. Shokhirev, E. N. Chin, L. L. Lairson, B. Melillo, S. L. Schreiber, S. Forli, J. R. Teijaro, B. F. Cravatt, *Cell* **2020**, *182*, 1009–1026.e29.
- [19] M. E. Abbasov, M. E. Kavanagh, T.-A. Ichu, M. R. Lazear, Y. Tao, V. M. Crowley, C. W. Am Ende, S. M. Hacker, J. Ho, M. M. Dix, R. Suci, M. M. Hayward, L. L. Kiessling, B. F. Cravatt, *Nat. Chem.* **2021**, *13*, 1081–1092.
- [20] J. N. Spradlin, E. Zhang, D. K. Nomura, *Acc. Chem. Res.* **2021**, *54*, 1801–1813.
- [21] L. Boike, A. G. Cioffi, F. C. Majewski, J. Co, N. J. Henning, M. D. Jones, G. Liu, J. M. McKenna, J. A. Tallarico, M. Schirle, D. K. Nomura, *Cell Chem. Biol.* **2021**, *28*, 4–13.e17.
- [22] F. A. Gowans, N. Forte, J. Hatcher, O. W. Huang, Y. Wang, B. E. Altamirano Poblano, I. E. Wertz, D. K. Nomura, *J. Am. Chem. Soc.* **2024**, *146*, 16856–16865.
- [23] S. J. Won, Y. Zhang, C. J. Reinhardt, L. M. Hargis, N. S. MacRae, K. E. DeMeester, E. Njomen, J. R. Remsberg, B. Melillo, B. F. Cravatt, M. A. Erb, *Mol. Cell* **2024**, *84*, 4125–4141.e10.
- [24] M. Takahashi, H. B. Chong, S. Zhang, T.-Y. Yang, M. J. Lazarov, S. Harry, M. Maynard, B. Hilbert, R. D. White, H. E. Murrey, C.-C. Tsou, K. Vordermark, J. Assaad, M. Gohar, B. R. Dürr, M. Richter, H. Patel, G. Kryukov, N. Brooijmans, A. S. O. Alghali, K. Rubio, A. Villanueva, J. Zhang, M. Ge, F. Makram, H. Griesshaber, D. Harrison, A.-S. Koglin, S. Ojeda, B. Karakyriakou, et al., *Cell* **2024**, *187*, 2536–2556.e30.
- [25] M. Kuljanin, D. C. Mitchell, D. K. Schweppe, A. S. Gikandi, D. P. Nusinow, N. J. Bulloch, E. V. Vinogradova, D. L. Wilson, E. T. Kool, J. D. Mancias, B. F. Cravatt, S. P. Gygi, *Nat. Biotechnol.* **2021**, *39*, 630–641.
- [26] M. Fan, W. Lu, J. Che, N. P. Kwiatkowski, Y. Gao, H.-S. Seo, S. B. Ficarro, P. C. Gokhale, Y. Liu, E. A. Geffken, J. Lakhani, K. Song, M. Kuljanin, W. Ji, J. Jiang, Z. He, J. Tse, A. S. Boghossian, M. G. Rees, M. M. Ronan, J. A. Roth, J. D. Mancias, J. A. Marto, S. Dhe-Paganon, T. Zhang, N. S. Gray, *eLife* **2022**, *11*, e78810.
- [27] M. R. Lazear, J. R. Remsberg, M. G. Jaeger, K. Rothamel, H.-L. Her, K. E. DeMeester, E. Njomen, S. J. Hogg, J. Rahman, L. R. Whitby, S. J. Won, M. A. Schafroth, D. Ogasawara, M. Yokoyama, G. L. Lindsey, H. Li, J. Germain, S. Barbas, J. Vaughan, T. W. Hanigan, V. F. Vartabedian, C. J. Reinhardt, M. M. Dix, S. J. Koo, I. Heo, J. R. Teijaro, G. M. Simon, B. Ghosh, O. Abdel-Wahab, K. Ahn, et al., *Mol. Cell* **2023**, *83*, 1725–1742.e12.
- [28] K. A. Scott, H. Kojima, N. Ropek, C. D. Warren, T. L. Zhang, S. J. Hogg, H. Sanford, C. Webster, X. Zhang, J. Rahman, B. Melillo, B. F. Cravatt, J. Lyu, O. Abdel-Wahab, E. V. Vinogradova, *Cell Chem. Biol.* **2025**, *32*, 201–218.e17.
- [29] D. Ogasawara, D. B. Konrad, Z. Y. Tan, K. L. Carey, J. Luo, S. J. Won, H. Li, T. R. Carter, K. E. DeMeester, E. Njomen, S. L. Schreiber, R. J. Xavier, B. Melillo, B. F. Cravatt, *Cell Chem. Biol.* **2024**, *31*, 2138–2155.e32.
- [30] Z. Liu, J. R. Remsberg, H. Li, E. Njomen, K. E. DeMeester, Y. Tao, G. Xia, R. E. Hayward, M. Yoo, T. Nguyen, G. M. Simon, S. L. Schreiber, B. Melillo, B. F. Cravatt, *J. Am. Chem. Soc.* **2024**, *146*, 10393–10406.
- [31] E. Njomen, R. E. Hayward, K. E. DeMeester, D. Ogasawara, M. M. Dix, T. Nguyen, P. Ashby, G. M. Simon, S. L. Schreiber, B. Melillo, B. F. Cravatt, *Nat. Chem.* **2024**, *16*, 1592–1604.
- [32] S. Hajra, S. M. Aziz, B. Jana, P. Mahish, D. Das, *Org. Lett.* **2016**, *18*, 532–535.
- [33] Y. M. Khetmalis, M. Shivani, S. Murugesan, K. V. G. Chandra Sekhar, *Biomed. Pharmacother. Biomedicine Pharmacother.* **2021**, *141*, 111842.
- [34] B. Yu, D.-Q. Yu, H.-M. Liu, *Eur. J. Med. Chem.* **2015**, *97*, 673–698.
- [35] M. Kaur, M. Singh, N. Chadha, O. Silakari, *Eur. J. Med. Chem.* **2016**, *123*, 858–894.
- [36] J. J. Badillo, N. V. Hanhan, A. K. Franz, *Curr. Opin. Drug Discov. Devel.* **2010**, *13*, 758–776.
- [37] A. J. Boddy, J. A. Bull, *Org. Chem. Front.* **2021**, *8*, 1026–1084.
- [38] S. Hajra, S. Singha Roy, S. M. Aziz, D. Das, *Org. Lett.* **2017**, *19*, 4082–4085.
- [39] S. Hajra, S. Singha Roy, A. Biswas, S. A. Saleh, *J. Org. Chem.* **2018**, *83*, 3633–3644.
- [40] N. Ma, J. Hu, Z.-M. Zhang, W. Liu, M. Huang, Y. Fan, X. Yin, J. Wang, K. Ding, W. Ye, Z. Li, *J. Am. Chem. Soc.* **2020**, *142*, 6051–6059.
- [41] L. Jiang, M. Menard, C. Weller, Z. Wang, L. Burnett, I. Aronchik, S. Steele, M. Flagella, R. Zhao, J. W. W. Evans, S. Chin, K.-J. Chou, Y. Mu, M. Longhi, L. McDowell, J. E. Knox, A. Gill, J. A. Smith, M. Singh, E. Quintana, J. Jiang, *Cancer Res.* **2023**, *83*, 526.
- [42] Y. Shibata, M. Chiba, *Drug Metab Dispos* **2015**, *43*, 375–384.
- [43] H. Yamada, T. Yoshida, H. Sakamoto, M. Terada, T. Sugimura, *Biochem. Biophys. Res. Commun.* **1986**, *140*, 167–173.
- [44] D. Talwar, C. G. Miller, J. Grossmann, L. Szyrwił, T. Schwecke, V. Demichev, A.-M. Mikecin Drazic, A. Mayakonda, P. Lutsik, C. Veith, M. D. Milsom, K. Müller-Decker, M. Müllleder, M. Ralsler, T. P. Dick, *Nat. Metab.* **2023**, *5*, 660–676.

- [45] C. J. Gerry, S. L. Schreiber, *Nat. Chem. Biol.* **2020**, *16*, 369–378.
- [46] N. London, *Chem. Rev.* **2024**, *125*, 326–368.
- [47] P. R. A. Zanon, F. Yu, P. Musacchio, L. Lewald, M. Zollo, K. Krauskopf, D. Mrdović, P. Raunft, T. E. Maher, M. Cigler, C. Chang, K. Lang, F. D. Toste, A. I. Nesvizhskii, S. M. Hacker, “Profiling the proteome-wide selectivity of diverse electrophiles” **2021**, <https://doi.org/10.33774/chemrxiv-2021-w7rss-v2>.
- [48] M. Varadi, S. Anyango, M. Deshpande, S. Nair, C. Natassia, G. Yordanova, D. Yuan, O. Stroe, G. Wood, A. Laydon, A. Žídek, T. Green, K. Tunyasuvunakool, S. Petersen, J. Jumper, E. Clancy, R. Green, A. Vora, M. Lutfi, M. Figurnov, A. Cowie, N. Hobbs, P. Kohli, G. Kleywegt, E. Birney, D. Hassabis, S. Velankar, *Nucleic Acids Res.* **2022**, *50*, D439–D444.
- [49] J. Jumper, R. Evans, A. Pritzel, T. Green, M. Figurnov, O. Ronneberger, K. Tunyasuvunakool, R. Bates, A. Žídek, A. Potapenko, A. Bridgland, C. Meyer, S. A. A. Kohl, A. J. Ballard, A. Cowie, B. Romera-Paredes, S. Nikolov, R. Jain, J. Adler, T. Back, S. Petersen, D. Reiman, E. Clancy, M. Zielinski, M. Steinegger, M. Pacholska, T. Berghammer, S. Bodenstein, D. Silver, O. Vinyals, et al., *Nature* **2021**, *596*, 583–589.
- [50] K. G. Mark, S. Kolla, J. D. Aguirre, D. M. Garshott, S. Schmitt, D. L. Haakonsen, C. Xu, L. Kater, G. Kempf, B. Martínez-González, D. Akopian, S. K. See, N. H. Thomä, M. Rapé, *Cell* **2023**, *186*, 3460–3475.e23.
- [51] A. R. Julio, F. Shikwana, C. Truong, N. R. Burton, E. R. Dominguez, A. C. Turmon, J. Cao, K. M. Backus, *Nat. Chem. Biol.* **2024**, *21*, 693–705.
- [52] W. L. Labisso, M. Wirth, N. Stojanovic, R. H. Stauber, A. Schnieke, R. M. Schmid, O. H. Krämer, D. Saur, G. Schneider, *Cell Cycle Georget. Tex.* **2012**, *11*, 1593–1602.

Manuscript received: May 05, 2025

Revised manuscript received: September 19, 2025

Manuscript accepted: September 22, 2025

Version of record online: September 25, 2025